Journal of Nuclear Materials 407 (2010) 137–142

Contents lists available at ScienceDirect

Journal of Nuclear Materials

journal homepage: www.elsevier.com/locate/jnucmat

Irradiation of synthetic garnet by heavy ions and α-decay of ^{244}Cm

Jiaming Zhang [a], Tatiana S. Livshits [b], Andrey A. Lizin [c], Qiaona Hu [a], Rodney C. Ewing [a,*]

[a] Department of Geological Sciences, University of Michigan, Ann Arbor, MI 48109-1005, USA
[b] Institute of Geology of Ore Deposits, Petrography, Mineralogy, and Geochemistry, Russian Academy of Sciences, Moscow 119017, Russia
[c] Research Institute of Atomic Reactors, Dimitrovgrad-10, 433512, Russia

ARTICLE INFO

Article history:
Received 5 August 2010
Accepted 23 September 2010

ABSTRACT

Garnet, $A_3B_2X_3O_{12}$, has a structure that can incorporate actinides. Hence, the susceptibility of the garnet structure to radiation damage has been investigated by comparing the results of self-radiation damage from α-decay of ^{244}Cm and a 1 MeV Kr^{2+} ion irradiation. Gradual amorphization with increasing fluence was observed by X-ray diffraction analysis and *in situ* transmission electron microscopy. The critical dose, D_c, for an yttrium–aluminum garnet ($Y_3Al_5O_{12}$) doped with 3 wt.% ^{244}Cm is calculated to be 0.4 displacements per atom (dpa). While the doses obtained by ion irradiation experiments of garnets with different compositions $(Y_{2.43}Nd_{0.57})(Al_{4.43}Si_{0.44})O_{12}$, $(Ca_{1.64}Ce_{0.41}Nd_{0.42}La_{0.18}Pr_{0.18}Sm_{0.14}Gd_{0.04})Zr_{1.27}Fe_{3.71}O_{12}$, and $(Ca_{1.09}Gd_{1.23}Ce_{0.43})Sn_{1.16}Fe_{3.84}O_{12}$, varied from 0.29 to 0.55 dpa at room temperature. The similarity in the amorphization dose at room temperature and critical temperature of the different garnet compositions suggest that the radiation response for the garnet structure is structurally constrained, rather than sensitive to composition, which is the case for the pyrochlore structure-type.

1. Introduction

Immobilization of long-lived actinides, e.g., ^{239}Pu and ^{237}Np, into durable crystalline phases is an essential aspect of the isolation of actinides from the biosphere [1–8]. However, of critical importance is the effect of the α-decay of the incorporated actinide on the periodic structure of the crystalline phase [9]. Radiation effects can be studied by a number of different methods [9]. As an example, minerals with Th and U sustain radiation damage as a function of actinide content and age, and their damaged microstructure, as a function of increasing dose, can be used to evaluate very long term effects [10,11]. However, a lack of knowledge of the thermal history of the natural samples limits the quantitative interpretation of damage and annealing mechanisms. Radiation damage processes may be accelerated using either ion beam irradiations [12–21] or doping of synthetic samples with highly active actinides (e.g., ^{238}Pu or ^{244}Cm) [22–25]. These studies can be completed as a function of fluence, temperature and variations in the composition of the structure-type. Although the dose rates for the ion beam experiments are much greater than for the actinide-doping experiments, it has been demonstrated that comparable doses for amorphization are obtained by both techniques [22]. In fact, all three approaches are required in order to estimate the damage accumulation in an actinide waste form [12]. In this study, we use the results of ion beam irradiation and ^{244}Cm-doping of the garnet structure in order to obtain direct information of the damage accumulation process and compare these results to data on U-bearing garnets recently discovered in the northern Caucasus of Russia [26].

Garnet, $A_3B_2(XO_4)_3$ (*Ia*3*d*, *Z* = 8), is an important group of minerals that have a wide range of compositions. Three cation sites A, B, and X with coordination numbers of 8, 6, and 4, respectively, provide structural sites for the incorporation of a variety of elements (Fig. 1). The $[A]^{VIII}$ site normally accommodates divalent (Ca, Mn, Mg, Fe, Co, Cd), trivalent (Y, REE, An), and tetravalent (An = Th, U, Pu, Np, Am) cations. Trivalent (Fe, Al, Ga, Cr, Mn, In, Sc, V) and tetravalent (Zr, Ti, Sn) cations occupy the $[B]^{VI}$ site. The $[X]^{IV}$ site can be occupied by trivalent (Al, Ga, Fe), tetravalent (Ge, Si, Ti), and pentavalent (V, As) cations [7,27]. The garnet structure can be synthesized with high concentrations of actinide and lanthanide elements, i.e., a synthetic garnet with (mainly Ca–Zr–Fe) has been shown to incorporate 18 wt.% uranium [28]. Recently, a new natural uranian garnet, elbrusite–(Zr) $Ca_3(U^{6+}Zr)(Fe_2^{3+}Fe^{2+})O_{12}$, with uranium contents up to 27 wt.% UO_3 has been discovered from the upper Chegem caldera, Northern Caucasus, Russia [26]. Thus, the garnet structure is an ideal candidate for the incorporation of actinides.

Yttrium aluminum garnet (YAG), $Y_3Al_5O_{12}$, was doped with 3 wt.% ^{244}Cm, and the effect of self-radiation damage from α-decay was determined as a function of cumulative dose. The decay of

* Corresponding author.
E-mail address: rodewing@umich.edu (R.C. Ewing).

0022-3115/$ - see front matter © 2010 Elsevier B.V. All rights reserved.
doi:10.1016/j.jnucmat.2010.09.051

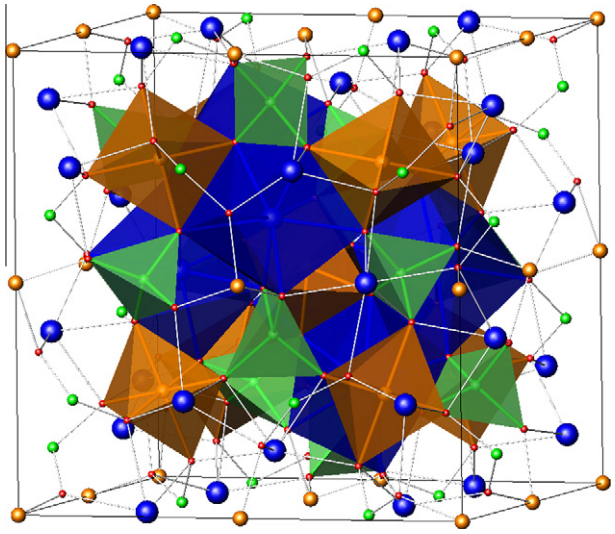

Fig. 1. Unit cell of garnet, $A_3B_2(XO_4)_3$ (*Ia3d*, $Z = 8$), viewed along [1 0 0]. The blue polyhedra are the 8-coordinated A-site cations, the yellow octahedra are the B-site cations, and the green tetrahedra are the X-site cations. The red spheres indicate the location of the oxygen. (For interpretation of the references to colour in this figure legend, the reader is referred to the web version of this article.)

^{244}Cm produces a 5.8 MeV α-particle and a 96 keV ^{240}Pu recoil nucleus [1]. The radiation response of the garnet structure is compared to 1 MeV Kr^{2+} ion irradiation of synthetic garnets with three different compositions: $(Y_{2.43}Nd_{0.57})(Al_{4.43}Si_{0.44})O_{12}$ [#G-15-3], $(Ca_{1.64}Ce_{0.41}Nd_{0.42}La_{0.18}Pr_{0.18}Sm_{0.14}Gd_{0.04})Zr_{1.27}Fe_{3.71}O_{12}$ [#G-1], and $(Ca_{1.09}Gd_{1.23}Ce_{0.43})Sn_{1.16}Fe_{3.84}O_{12}$ [#Sn-1]. By characterizing the microstructural evolution upon ion irradiation at temperatures ranging from 298 to 823 K using *in situ* transmission electron microscopy, the radiation response of garnet matrices with complex compositions can be investigated.

2. Experimental methods

2.1. Sample synthesis

The garnet samples were synthesized by cold pressing (200 MPa) of stoichiometric mixtures of the constituent oxides followed by sintering in air at 1300–1500 °C for 5 h [28]. Three chemical compositions of the garnets (listed in Table 1), $(Y_{2.43}Nd_{0.57})(Al_{4.43}Si_{0.44})O_{12}$ [#G-15-3], $(Ca_{1.64}Ce_{0.41}Nd_{0.42}La_{0.18}Pr_{0.18}Sm_{0.14}Gd_{0.04})Zr_{1.27}Fe_{3.71}O_{12}$ [#G-1], and $(Ca_{1.09}Gd_{1.23}Ce_{0.43})Sn_{1.16}Fe_{3.84}O_{12}$ [#Sn-1], were selected for ion beam irradiation experiments. Crystal structure and chemical composition analysis of the garnet samples by different analytical methods were completed at the Institute of Geology of Ore Deposits (Moscow, Russia). The crystal structure was determined by X-ray diffraction (XRD) analysis using a Rigaku D/Max 2200 diffractometer (Cu Kα irradiation, voltage 40 keV, current 20–30 mA, 2θ angular range 2–60° with a step of 0.01–0.02°). Phase compositions were determined on a JSM 5300 SEM with an INCA-4500 EDS (voltage 25 keV, current 1 nA, beam diameter 3–5 μm, pulse collection time 100 s; oxides and fluorides are used as standards).

Table 1
Compositions (wt.%) and formulas of garnets with analogs of the An-REE fraction of HLW in the samples for IVEM irradiation and ^{244}Cm-doped sample.

#	Compositions				
$(Y_{2.43}Nd_{0.57})(Al_{4.43}Si_{0.44})O_{12}$					
G-15-3	Al_2O_3	SiO_2	Y_2O_3	Nd_2O_3	
	36.2	4.2	44.1	15.4	

$(Ca_{1.64}Ce_{0.41}Nd_{0.42}La_{0.18}Pr_{0.18}Sm_{0.14}Gd_{0.04})Zr_{1.27}Fe_{3.71}O_{12}$									
G-1	CaO	La_2O_3	Pr_2O_3	Nd_2O_3	Sm_2O_3	Gd_2O_3	CeO_2	ZrO_2	Fe_2O_3
	11.8	3.7	3.8	9.0	3.0	1.0	9.0	20.0	38.0

$(Ca_{1.09}Gd_{1.23}Ce_{0.43})Sn_{1.16}Fe_{3.84}O_{12}$					
Sn-1	CaO	Fe_2O_3	Gd_2O_3	CeO_2	SnO_2
	7.1	35.7	20.3	9.7	26.2

$Y_{2.89}Cm_{0.1}Pu_{0.01}Al_5O_{12}$				
Y-Cm	Al_2O_3	Cm_2O_3	Y_2O_3	PuO_2
	41.7	4.2	53.4	0.4

Aluminate garnet (#Y-Cm) with bulk composition $Y_{2.88}Cm_{0.12}Al_5O_{12}$, doped with 3 wt.% ^{244}Cm ($T_{1/2}$ = 18 years), was synthesized in order to investigate the effects of α-decay damage. The distribution of Cm in the garnet was investigated by a study of its surrogate element, Sm. The garnet was synthesized by solid state reaction of Y_2O_3, Sm_2O_3, and Al_2O_3 mixture (pressing and then sintering at 1400 °C over 4 h), and a maximum of 15 wt.% of Sm can be incorporated in this yttrium aluminate garnet (with formula $Y_{2.44}Sm_{0.56}Al_{4.62}Si_{0.28}O_{12}$) [29]. Initial Cm used for sample preparation contained not only ^{244}Cm (75% of total Cm), but also long-lived ^{245}Cm and ^{248}Cm (25%) and also ^{240}Pu (0.36 wt.%). The final calculated composition of garnet is: $Y_{2.89}Cm_{0.1}Pu_{0.01}Al_5O_{12}$. The synthesis and investigation of the Cm-doped samples were completed at the Institute of Atomic Reactors (Dimitrovgrad, Russia).

2.2. Ion beam irradiation

The thin foils of specimens on TEM grids were irradiated by 1-MeV Kr^{2+} ions at temperatures ranging from room temperature to 873 K and observed by *in situ* TEM using the IVEM-Tandem Facility at the Argonne National Laboratory. A constant ion flux of 6.25×10^{14} ions/m^2 s was used during the irradiation. Selected area electron diffraction (SAED) patterns were used to monitor the amorphization process during the intervals of increasing ion dose. The critical amorphization fluence, at which complete amorphization occurs, was determined by the disappearance of all of the diffraction maxima in the SAED patterns. The critical amorphization fluence has been converted into a unit of displacements per atom (dpa) and also to the kinetic energy transferred to each target atom through nuclear collision (E_n) using SRIM-2008 simulations [30]. The equations for the conversion are:

$$\text{dpa} = \frac{F_c \times [\text{displacements by single ion per Å}] \times 10^8}{\text{atomic density}} \quad (1)$$

$$E_n = \frac{E_n' \times F_c \times 10^8}{\text{atomic density}} \quad (2)$$

$$E_n' = E_R - I_R + P_I \quad (3)$$

where E_R, I_R, and P_I are the ion energy loss to recoil atoms, the recoil ionization energy, and the incident ion energy loss to phonons, respectively. These values were obtained from the average of damage profile assuming the TEM sample thickness to be approximately 100 nm. The displacement threshold energies (E_d) of Zr and O used in the calculation were 79 and 47 eV, respectively [31]. The E_d for other cations was assumed to be 25 eV.

2.3. Cm-doped garnet

The structural damage caused by α-decay events accumulated progressively with increasing of time and hence irradiation dose. The Cm-doped sample (#Y-Cm) was examined periodically by

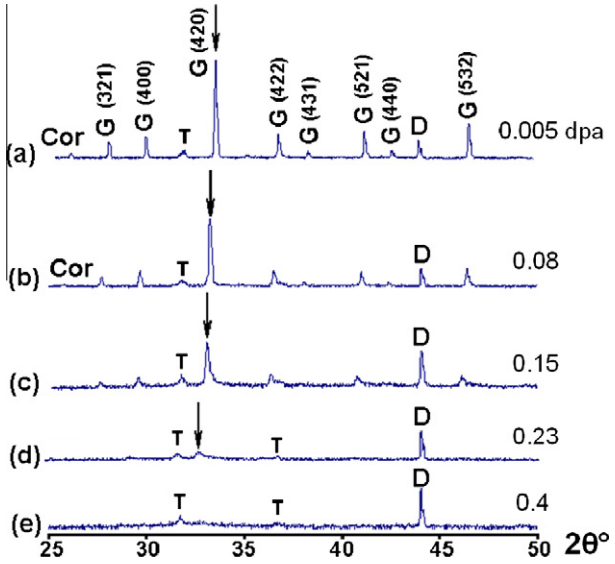

Fig. 2. Changes of XRD patterns of Cm-doped garnet as a function of increasing dose (dpa). G – garnet, Cor – corundum, T – Teflon (germetizaion of sample for XRD investigations), D – diamond (standard). Data from Livshits et al. [29].

XRD. The XRD data show that garnet with unit cell parameter 1.20140 (7) nm prevails in the sample #Y-Cm (shown in Fig. 2). There is small amount of corundum in matrix. There were also a few diffraction peaks from Teflon and diamond in the XRD patterns. Teflon and diamond were used in the XRD investigations of the sample: the Teflon for sealing the ceramic and the diamond as a standard.

The critical dose value (D_c) was calculated using formula:

$$D = {}^{244}N_0 \times \left(1 - e^{-\lambda_{244} t}\right), \quad (4)$$

where ${}^{244}N_0$ – initial concentration of ^{244}Cm (number of molecule/g), λ – decay constant of ^{244}Cm ($\ln 2/T_{1/2}$) and t – time of experiment (18 months). Amorphization dose in dpa was calculated using the following equation:

$$d = (1372 \times D \times M)/(N_f \times N_A), \quad (5)$$

where D = dose in decays/g, M = garnet molecular mass, N_f = 20 (number of atoms in garnet formula), N_A = Avogadro constant, the average number of displacements between alpha-particles, recoil nuclei and structural atoms during a single alpha-decay event is 1372 calculated using SRIM-2008 simulations [30] (this number is approximately the same as the 1500 displacements used in Ref. [32]).

3. Results and discussion

Fig. 2 shows the X-ray diffraction patterns of Cm-doped sample (#Y-Cm) as function of time corresponding to increasing dose (dpa). There are several significant changes in the XRD patterns with increasing time and dose: the intensity of garnet diffraction maxima decreases, the peaks broaden, and lower intensity diffraction maxima disappear. Garnet peaks are shifted to lower 2θ values due to expansion of the unit cell as isolated defects accumulate in the structure. The volume expansion of garnet unit cell is calculated to be ~2.1% at a dose of 0.19 dpa (Fig. 2d). Observed changes of XRD patterns are due to the accumulation of radiation-induced damage in the garnet structure, which results from interactions between atoms of garnet structure and the α-decay event (α-particles and mainly the α-recoil nuclei). The D_c for aluminate garnet is 4.25×10^{18} α-decays/g or 0.4 dpa.

The characteristic of crystalline-to-amorphous transition in the garnet structure upon ion irradiation, as observed by TEM, is shown in Fig. 3 for #G-15-3. Below the critical amorphization temperature (T_c), the amorphization process occurs gradually with increasing ion dose due to the accumulation of amorphous domains caused by collision cascade (i.e., at 298 and 473 K), which is consistent with previous observations [33,34]. The very similar amorphization dose for garnet irradiated along [1 0 1] and [1 1 1] indicates that the damage mechanism is not affected by crystallographic orientation, as garnet is isometric. Above the critical temperature (T_c = 823 K for #G-15-3), the critical amorphization dose increases to infinity and complete amorphization does not occur (Fig. 4). Similarly, *in situ* SAED patterns and HRTEM images of #G-1 before and after irradiation (Fig. 5) showed that there is no

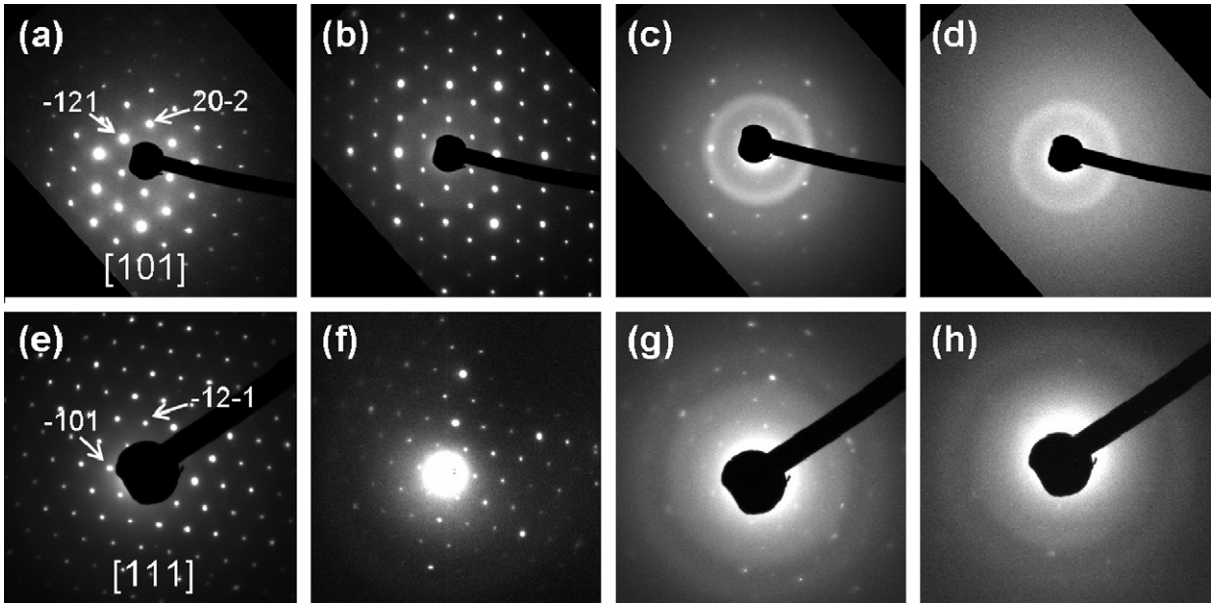

Fig. 3. Changes of SAED patterns of G-15-3 garnet irradiated by 1 MeV Kr^{2+} at 298 K: (a) unirradiated; (b) 0.22 dpa; (c) 0.44 dpa; (d) 0.55 dpa; at 473 K (e) unirradiated; (f) 0.22 dpa; (g) 0.44 dpa; (h) 0.55 dpa.

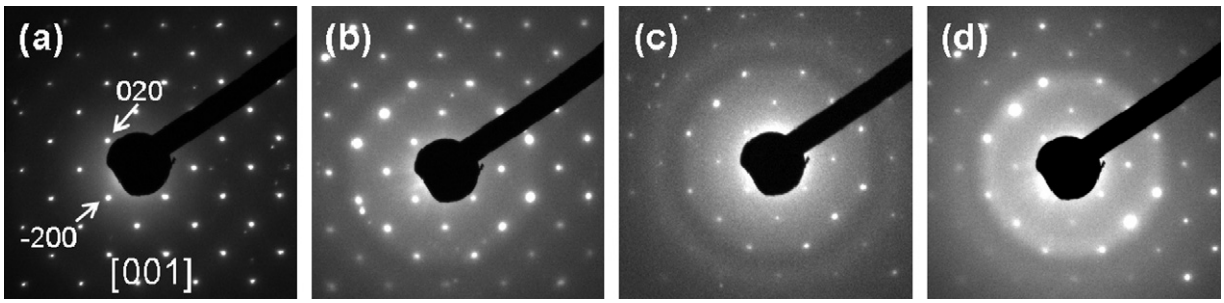

Fig. 4. Sequences of SAED patterns of G-15-3 garnet irradiated by 1 MeV Kr^{2+} did not change at 823 K to the dose of (a) 0 dpa; (b) 0.88 dpa; (c) 1.925 dpa; (d) 2.75 dpa.

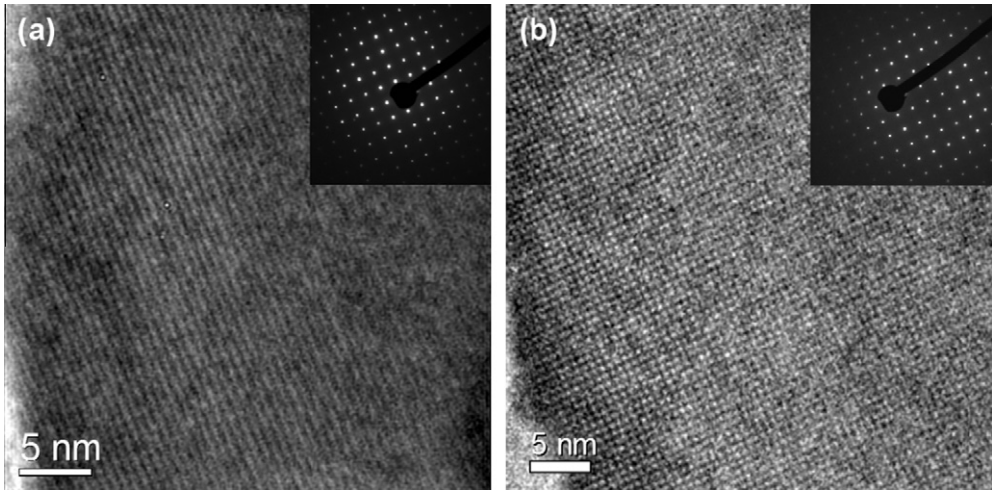

Fig. 5. SAED patterns and HRTEM images of G-1 garnet irradiated by 1 MeV Kr^{2+} at critical temperature (773 K) did not become amorphous as observed (a) unirradiated and (b) after 3.2 dpa.

change in the microstructure (e.g., formation of amorphous cascades or chemical decomposition) when the irradiation is completed at temperatures greater than the T_c.

The synthetic garnet structures have a unit cell parameter ranging from 1.21 to 1.28 nm based on measurements from SAED patterns. The theoretical density (listed in Table 2) was used to calculate the electronic and nuclear stopping power due to the 1 MeV Kr^{2+} ion irradiation. The calculated energy deposition by nuclear collision (dE/dx_n) and electron ionization process (dE/dx_e) have been determined using SRIM-2008 code and tabulated in Table 2. The electronic to nuclear stopping power (ENSP) ratio is 0.77 for #G-15-3 garnet, slightly greater than the #G-1 and #Sn-1 garnets. Table 3 compiles the amorphization fluence, critical dose and energy loss due to nuclear collision at different temperatures. The temperature dependence of D_c for the garnets in Fig. 6 shows an increase in amorphization dose at higher temperature. The solid symbols in Fig. 6 are for data measured at high temperatures, and these data indicate that the garnets did not amorphize at the indicated ion dose. The curves were obtained by fitting the data based on the model described in Ref. [35]. Generally, the greater the ratio of ENSP the lower T_c, as the ionization process resulting from electronic energy loss may lead to enhanced annealing of radiation-induced defects [36,37]. However, this trend is not consistent with the results for the garnet compositions investigated in this study. For instance, there is a 100 K difference between #G-1 and #Sn-1 garnets, although they have a similar ENSP ratio (0.70). Other parameters, such as defect migration energies [35] and the size of the subcascades that form in different compositions of the garnet structure [33,38], may be correlated to the variation

Table 2
Structural characterization of the garnets and stopping power calculated by SRIM-2008.

Samples	Unit cell parameter (nm)	Density (g/cm^3)	dE/dx_e	dE/dx_n	ENSP
G-15-3	1.21	4.69	964	1251	0.77
G-1	1.28	5.25	892	1276	0.70
Sn-1	1.26	5.45	907	1303	0.70

in T_c. Nevertheless, the three synthetic garnets exhibit a narrow range of T_c values (between 773 and 873 K), indicating that the radiation response of the garnet structure is largely constrained by the structure.

A comparative study of the radiation response on the natural and synthetic garnets with various compositions by ion beam irradiation has been completed by Utsunomiya et al. [33]. For the natural silicate garnets and synthetic ferrate–aluminate garnets, the critical amorphization doses ranged between 0.15 and 0.32 dpa at room temperature, and the critical temperature ranges from 890 to 1130 K [33]. Similarly, the critical amorphization dose of the synthetic ferrate garnets are between 0.17 and 0.19 dpa and the critical temperature varies from 820 to 870 K [34]. In the present study, the G-1 and Sn-1 garnets have Fe at the $[X]^{IV}$ site, so the critical amorphization dose and critical temperature are close to that of the ferrate garnet [34]. The #G-15-3 sample has Al and Si in the $[X]^{IV}$ site, with a relatively higher critical amorphization dose (0.55 dpa), but it has a similar critical temperature (823 K). The range in the susceptibilities of garnets of different composition to

Table 3
Values of amorphization dose (ions/m^2 and dpa) and energy loss by nuclear collision, E_n (eV/atom) at different temperatures. The value in bold is the critical temperature, T_c (K).

Samples	T (K)	F_c ($\times 10^{19}$ ions/m^2)	dpa	E_n
G-15-3				
$N_{collision}$ = 1.0	298	0.5	0.55	50.4
E_r = 160	473	0.56	0.62	56.5
I_r = 70	723	0.75	0.83	75.7
P_i = 1	**823 (T_c)**	2.5	2.75	252.2
G-1				
$N_{collision}$ = 1.1	298	0.26	0.37	27.2
E_r = 120	473	0.24	0.34	25.1
I_r = 40	673	0.3	0.43	31.4
P_i = 1	**773 (T_c)**	2.25	3.2	235.2
Sn-1				
$N_{collision}$ = 1.2	298	0.19	0.29	22.8
E_r = 160	473	0.25	0.38	30.0
I_r = 65	553	0.25	0.38	30.0
P_i = 1	748	0.8	1.2	96.1
	873 (T_c)	2.5	3.75	300.4

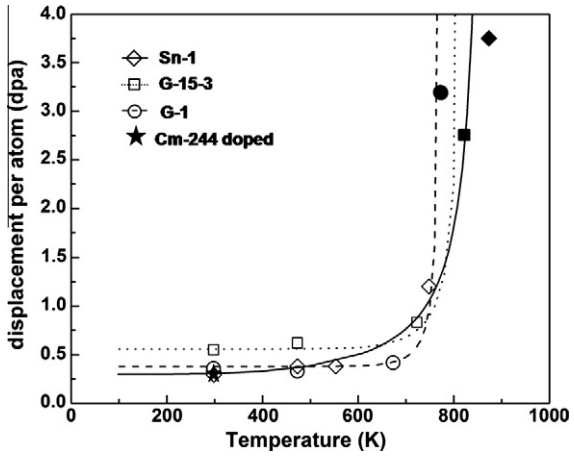

Fig. 6. Temperature dependence of radiation-induced amorphization doses (dpa) for the garnet structure as a result of ion irradiation and the α-decay of ^{244}Cm. The solid symbols measured at high temperatures indicate that the garnets did not amorphize at the indicated ion dose, which are significantly higher than the amorphization doses at the room temperature. (For interpretation of the references to colour in this figure legend, the reader is referred to the web version of this article.)

radiation damage appears to be minimal; thus, the susceptibility of the garnet structure to radiation damage is mainly controlled by its structural topology, that is the degrees of freedom, *f*, in the structure [39,40]. As previously analyzed, the degrees of freedom for structural rearrangement in garnet are comparable to that of the zircon structure, and the dose for amorphization at room temperature for zircon and the different garnet compositions are also similar. Although changes in amorphization dose for the isometric garnet structure do not vary much with composition, this is not the case for the isometric pyrochlore structure ($A_2B_2O_7$) [12–14]. In the latter case, cation and anion disordering of the pyrochlore structure plays a significant role in determining the final damage state [41]. Such structural disordering is not possible in the garnet structure.

In order to understand the radiation response of garnet to the α-decay event damage, ^{244}Cm was selected as an actinide dopant because of its short-half life (18.1 year) and very high specific activity. Generally, the damage rate that results from actinide doping is 10^{-10}–10^{-8} dpa/s, much lower than that obtained during ion beam irradiation, which is 10^{-5}–10^{-2} dpa/s [35]. Still, ion beam irradiation has proven to be an effective method for surveying the radiation response of a wide variety of materials and obtaining a fundamental understanding of the ballistic interactions caused by α-decay events. Previously, the comparison of ion beam damage and self-radiation damage from incorporated actinides has been completed for titanate pyrochlore, silicate apatite, and zircon. A synthetic pyrochlore, $Gd_2Ti_2O_7$, doped with 1.24 wt.% ^{244}Cm transforms to an amorphous state after a dose of 0.16 dpa (3.5×10^{18} α-decay/g), and a 1-MeV Kr^+ irradiation shows a similar dose for amorphization of 0.18 dpa [22]. While, some variation was found in ^{244}Cm-doped $Ca_2Nd_8(SiO_4)_6O_2$ apatite (D_c = 0.3 dpa) and 1.5 MeV Kr^+ (1.5 MeV Xe^+) irradiated $Ca_2La_8(SiO_4)_6O_2$ (D_c = 0.4–0.5 dpa) [42,43]. In addition, systematic studies of natural zircon, ^{238}Pu-doped zircon, and ion beam irradiated zircon have shown that all samples become amorphous at ~0.5 dpa [44]. Radiological nuclear magnetic resonance measurements on highly radioactive ^{239}Pu zircon show damage similar to that caused by ^{238}U and ^{232}Th in natural zircons at the same dose, indicating no significant effect of half-life or loading levels (i.e., dose rate effects) [25]. Results obtained in this investigation show good agreement between doses required for amorphization, D_c, and the critical temperature, T_c, for Cm-doped (0.4 dpa) and heavy ion irradiation (0.29–0.55 dpa) of the garnet structures.

4. Conclusions

The response of synthetic garnets with a variety of compositions to ion beam irradiation was investigated and compared to self-radiation damage caused by the α-decay in garnet doped with ^{244}Cm. Radiation-induced amorphization due to ion irradiation was observed for all garnet compositions below the critical temperature for amorphization (between 773 and 873 K). The ^{244}Cm-doped garnet became amorphous at 0.4 dpa, as compared to doses in the range of 0.29–0.55 dpa for ion beam irradiations. The small variation in the amorphization dose at room temperature and the generally consistent critical temperature for the garnets with different compositions suggest that the radiation response of the garnet structure is topologically constrained and not very sensitive to variations in composition.

Acknowledgements

We thank the staff of the IVEM-Tandem Facility at the Argonne National Laboratory for assistance with the irradiation experiments. This work was supported as part of the Materials Science of Actinides, an Energy Frontier Research Center funded by the US Department of Energy, Office of Basic Energy Sciences under Award Number DE-SC0001089. This study was partially supported by the Russian Foundation for Basic Research (Projects 08-05-00024-a).

References

[1] W.J. Weber, J.W. Wald, H.J. Matzke, J. Nucl. Mater. 138 (1986) 196.
[2] K.E. Sickafus, L. Minervini, R.W. Grimes, J.A. Valdez, M. Ishimaru, F. Li, K.J. McClellan, T. Hartmann, Science 289 (2000) 748.
[3] W.J. Weber, R.C. Ewing, Science 289 (2000) 2051.
[4] R.C. Ewing, Proc. Natl. Acad. Sci. 96 (7) (1999) 3432.
[5] N.P. Laverov, S.V. Yudintsev, S.V. Stefanovsky, J. Lian, R.C. Ewing, Doklady Russ. Acad. Sci. 376(5) (2001) 665–667 (in Russian) or Trans. Russ. Acad. Sci. Earth Sci. Sect. 377(pt. 2) (2001) 175–177 (in English).
[6] N.P. Laverov, S.V. Yudintsev, S.V. Stefanovsky, Y. Jang, M.I. Lapina, A.V. Sivtsov, R.C. Ewing, Doklady Akademii Nauk 385A (2002) 524–528; 671–675 (English translation).
[7] N.P. Laverov, S.V. Yudintsev, T.S. Ioudintseva, S.V. Stefanovsky, R.C. Ewing, J. Lian, Geol. Ore Deposits 45 (6) (2003) 423.

[8] N.P. Laverov, S.V. Yudintsev, T.S. Livshits, S.V. Stefanovsky, A.N. Lukinykn, R.C. Ewing, Geochimiya 48(1) (2010) 3–16 (in Russian); Geochem. Int. 48(1) (2010) 1–14 (Translation).
[9] R.C. Ewing, W.J. Weber, Actinide waste forms and radiation effects. In: R. Lester, Morss, Norman Edlestein, Jean Fuger (Eds.), The Chemistry of the Actinide and Transactinide Elements, vol. 6, Springer, Amsterdam, 2010, pp. 3813–3888.
[10] R.C. Ewing, R.F. Haaker, Nucl. Chem. Waste Manage. 1 (1980) 51.
[11] G.R. Lumpkin, R.C. Ewing, Phys. Chem. Miner. 16 (1988) 2.
[12] R.C. Ewing, W.J. Weber, J. Lian, J. Appl. Phys. 95 (2004) 5949.
[13] S.X. Wang, B.D. Begg, L.M. Wang, R.C. Ewing, W.J. Weber, K.V.G. Kutty, J. Mater. Res. 14 (1999) 4470.
[14] J. Lian, L.M. Wang, S.X. Wang, J. Chen, L.A. Boatner, R.C. Ewing, Phys. Rev. Lett. 87 (2001) 145901.
[15] J. Lian, X.T. Zu, K.V.G. Kutty, J. Chen, L.M. Wang, R.C. Ewing, Phys. Rev. B 66 (2002) 054108.
[16] J. Lian, J. Chen, L.M. Wang, R.C. Ewing, J.M. Farmer, L.A. Boatner, K.B. Helean, Phys. Rev. B 68 (2003) 134107.
[17] J. Lian, L.M. Wang, R.C. Ewing, L.A. Boatner, Nucl. Instrum. Meth. Phys. Res. B 241 (2005) 365.
[18] J. Lian, L.M. Wang, R.C. Ewing, S.V. Yudintsev, S.V. Stefanovsky, J. Appl. Phys. 97 (2005) 113536.
[19] J. Lian, K.B. Helean, B.J. Kennedy, L.M. Wang, A. Navrotsky, R.C. Ewing, J. Phys. Chem. B 110 (2006) 2343.
[20] J. Lian, J.M. Zhang, V. Pointeau, F.X. Zhang, M. Lang, F.Y. Lu, C. Poinssot, R.C. Ewing, J. Nucl. Mater. 393 (2009) 481.
[21] J.M. Zhang, J. Lian, A. Fuentes, F.X. Zhang, M. Lang, F.Y. Lu, R.C. Ewing, Appl. Phys. Lett. 94 (2009) 243110.
[22] W.J. Weber, J.W. Wald, Hj. Matzke, Mater. Lett. 3 (1985) 173.
[23] W.J. Weber, J. Am. Ceram. Soc. 76 (1993) 1729.
[24] W.J. Weber, Radiat. Eff. Defects Solids 115 (1991) 341.
[25] I. Farnan, H. Cho, W.J. Weber, Nature 445 (2007) 190.
[26] I.O. Galuskina, E.V. Galuskin, T. Armbruster, B. Lazic, J. Kusz, P. Dzierzanowski, V.M. Gazeev, N.N. Pertsev, K. Prusik, A.E. Zadov, A. Winiarski, R. Wrzalik, A.G. Gurbanov, Am. Mineral. 95 (2010) 1172.
[27] K.R. Whittle, G.R. Lumpkin, F.J. Berry, G. Oates, K.L. Smith, S. Yudintsev, N.J. Zaluzec, J. Solid State Chem. 180 (2007) 785.
[28] S. Yudintsev, M. Lapina, T. Yudintseva, S. Utsunomiya, L.M. Wang, R.C. Ewing, Mater. Res. Soc. Symp. Proc. 713 (2002) 477.
[29] T.S. Livshits, A.A. Lizin, J. Zhang, R.C. Ewing, Geol. Ore Deposits. 52 (2010) 543.
[30] SRIM, 2008. <http://www.srim.org/SRIM/SRIM2008.htm>.
[31] R.E. Williford, R. Devanathan, W.J. Weber, Nucl. Instrum. Meth. Phys. Res. B 141 (1998) 94.
[32] G.R. Lumpkin, B.C. Chakoumakos, R.C. Ewing, Am. Mineral. 71 (1986) 569.
[33] S. Utsunomiya, S. Yudintsev, L.M. Wang, R.C. Ewing, J. Nucl. Mater. 303 (2002) 177.
[34] S. Utsunomiya, S. Yudintsev, R.C. Ewing, J. Nucl. Mater. 336 (2005) 251.
[35] W.J. Weber, R.C. Ewing, C.R.A. Catlow, T. Diaz de la Rubia, L.W. Hobbs, C. Kinoshita, Hj. Matzke, A.T. Motta, M. Nastasi, E.K.H. Salje, E.R. Vance, S.J. Zinkle, J. Mater. Res. 13 (1998) 1434.
[36] S.J. Zinkle, J. Nucl. Mater. 219 (1995) 113.
[37] A. Meldrum, L.A. Boatner, R.C. Ewing, Phys. Rev. B 56 (1997) 13.
[38] S.X. Wang, L.M. Wang, R.C. Ewing, Phys. Rev. B 63 (2000) 024105-1.
[39] L.W. Hobbs, A.N. Sreeram, C.E. Jesurum, B.A. Berger, Nucl. Instrum. Meth. B 116 (1996) 18.
[40] L.W. Hobbs, Nucl. Instrum. Meth. B 91 (1994) 30.
[41] J.M. Zhang, J. Lian, F.X. Zhang, J.W. Wang, A. Fuentes, R.C. Ewing, J. Phys. Chem. C 114 (2010) 11810.
[42] W.J. Weber, Hj. Matzke, Mater. Lett. 5 (1986) 9.
[43] L.M. Wang, W.J. Weber, Phil. Mag. A 79 (1999) 237.
[44] W.J. Weber, R.C. Ewing, L.M. Wang, J. Mater. Res. 9 (1994) 688.